

Design and Testing of Wireless Motion Gauges for Two Collaborative Robot Arms

Yong-Sik Kim, Nicholas G. Dagalakis, Jeremy Marvel, Geraldine Cheok

*Intelligent Systems Division, Engineering Laboratory, National Institute of Standards and Technology,
100 Bureau Dr. Gaithersburg, MD, 20899, USA, yong@nist.gov*

Most existing robot performance evaluation methods focus on single robotic arms performing independent motion tasks. In this paper, a motion gauge is proposed to evaluate the symmetrical coordinated-motion performance between two robotic arms. For this evaluation, the proposed device monitors the relative distance between the two robotic arms in real-time, which is used to evaluate the coordinated-motion errors with respect to accuracy, and repeatability between the two arms. The proposed metrology device is composed of two linear displacement sensors sliding on a linear rail, two ball-and-socket magnetic couplers for mounting to robotic arms, and a wireless communication module for data transmission. For validation, the proposed system monitored the two robotic arms programmed to simulate symmetrical coordinated motions.

Keywords: Collaborative robots, symmetrical coordinated-motion, motion tracking, metrology-bar, robot performance evaluation.

1. INTRODUCTION

Commercial robots are becoming more integrated into our daily human lives, such as robotic cleaners at home [1], automatic drone delivery services [2], and collaborative robots in manufacturing [3]. As robots become more integrated with human environment, where many operations are designed to be executed by two arms, several robots have been designed to mimic these human two-arm operations. Examples of these types of operations in manufacturing are moving boxes or metal sheets, performing deburring of parts and several other similar operations that are better performed by two arms working together in a synchronized manner. Due to the nature of these applications, synchronized and coordinated-motion performance between the engaged robot arm pairs is important.

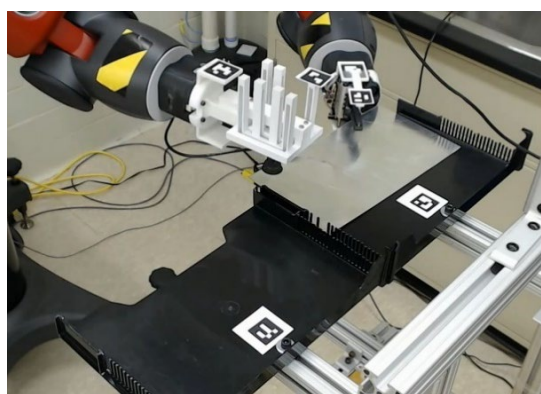
Multi robot arm manipulation can be categorized into coordinated and uncoordinated motions [4]. Uncoordinated motions are independent motions without considering other arms. In this case, each arm is programmed without considering the other, such as executing independent tasks in sequential order [5], [6]. Coordinated-motion tasks are those in which two or more arms need to be synchronized with each other to complete complex tasks [5], [6]. Coordinated-motion tasks are also divided into symmetrical and asymmetrical tasks. In asymmetrical tasks, each arm needs to manipulate different objects in a coordinated manner such as inserting a tool into a hole or fastening an object to another object. In this case, the position of the shared object is important. In

symmetrical tasks, two arms are controlled to manipulate the same object, such as moving a plate, as shown in Fig.1., or rotating a valve handle [7]. In this case, a closed kinematic chain is made between the two arms and a target object, which should be taken into consideration in robot control “for a successful operation.”

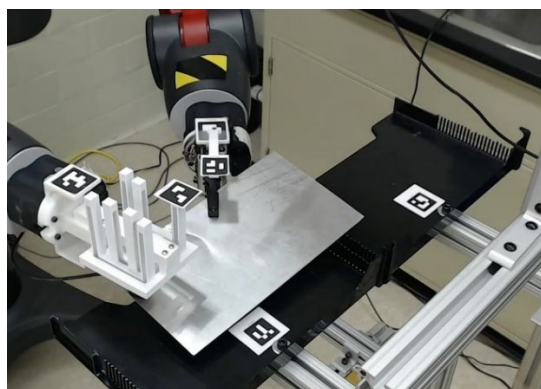
Coordinated-motion errors can cause the distance between the robot arms’ end effectors to change or can cause a motion time delay between them, resulting in slipping, losing contact, damaging the gripped object, etc. These coordinated-motion errors could be due to several factors: 1) motion errors from each arm, 2) time synchronization motion errors between the arms, 3) electromechanical defects (stiction, backlash encoder malfunction), 4) calibration errors, and 5) torque or force limits. Time synchronization errors could be due to: 1) different robot controllers, 2) different kinematic algorithms, 3) processing time differences, etc. The performance of symmetrical coordinated-motion tasks has been evaluated in various ways: 1) software simulation [5], [6], and 2) independent external sensors, such as laser trackers [9], [10], telescoping ball bars [11], [12], and motion-tracking systems [13], [14].

A laser tracker interferometer consists of a laser interferometer, a gimbal system, and a reflector. It can measure the three-dimensional (3D) position (X-Y-Z coordinates) of a target in real-time, based on the distance measured by its laser interferometer and the azimuth and elevation angles of the gimbals, which aim a laser beam at a

retroreflector attached to the target [10]. In one study, a Faro laser tracker¹ was used to measure the 3D coordinates of a target attached to a robot arm at five arm locations along a robot arm test path for performance evaluation [9]. This metrology system can monitor the 3D position of a single point of a single robotic arm with high accuracy, but it cannot track multiple arms simultaneously. For this reason, it is not very practical to use in the case of a two-arm coordinated-motions test.



a)



b)

Fig.1. The symmetrical coordinated motion task between two arms: a) gripping the plate, and b) moving the plate.

A telescoping ball bar is a physical ruler consisting of a center pivot assembly, a ball bar, extension bars, and a calibrator [11]. One end of the ball bar is attached to a pivot center, and the other end is attached to a robot arm. When the robot arm generates a circular motion around the pivot center, the sensor in the ball-bar system measures its length change [12]. This device is limited to measuring changes in length caused by rotational motions alone, and only over a short measurable range of a few mm.

A vision-based motion-tracking system measures the 3D position of fiducial markers by analyzing images captured from multiple cameras [13]. It uses vision cameras or sensors and special targets, forming a motion-tracking system that can track multiple targets with sub-millimeter-level accuracy at a rate of 40 to 120 frames per second [13]. Since this system uses multiple optical cameras or visual sensors, it is necessary to void occlusions and reduce image noise caused by cluttered scenes. In addition, post-processing is needed to extract

meaningful target data from the detected fiducial markers and to calculate the position and orientation of the robot arms from data collected at multiple detected targets [14]. In addition, micro-electro-mechanical systems (MEMS) based accelerometers or position sensors can also be used in positioning the robotic arms. They are inexpensive, so they provide low-cost performance. However, low-cost MEMS accelerometers tend to experience drift and it is difficult to achieve the necessary performance measurement accuracy for robots with currently commercially available MEMS sensors.

In this paper, a new metrology system is proposed to directly measure the performance of symmetrical coordinated motions executed by robot arms. This metrology system is compact and portable to use and operates through wireless data communication, which makes it possible to monitor two robot arms without any interference or limitations from the space around the robots. The design, fabrication, calibration, testing, and use of the proposed metrology system are described in the following sections.

2. SUBJECT & METHODS

The basic design of the proposed motion gauge is described as linear rail rods with two mounting modules, as shown in the schematic drawing of Fig.2.a. The two modules can be moved on the linear rail and secured to any desired location based on the robot testing needs. A coupling socket three-degrees-of-freedom (3-DOF) rotational joint in each of these modules can slide on the linear rail, and during testing will be attached to the two robotic arms to measure their motion displacements. A linear displacement sensor is connected to the sliding segment of each coupling socket and measures the mounted arm motion displacements within designated range B. From the measured displacements of the two arms, it is possible to determine the distance between them in real-time within a designated distance range A of the two modules. The distance A can be the default minimum distance between the two robotic arms and depends on the geometric design of the two robot arms. The linear sensors in the modules monitor the displacement of the two robot arms when they slide along the linear rail. For our current gauge design, a linear potentiometer was selected as a linear displacement sensor because of its simplicity and affordable price. Optical or magnetic linear encoder sensors, or linear voltage differential transducer (LVDT) sensors, etc., could also be used.

The 3D images of the motion gauge, the two modules, the 3-DOF sockets, and the linear potentiometers for the two robot arms are shown in Fig.2.b and Fig.2.c. The 3-DOF sockets work as rotational joints that transfer the linear motions relevant to the distance between the two robot arms to the linear potentiometers and filter off any rotational motions irrelevant to the distance. Since many commercial robotic arms provide six or seven DOF motions, any kinematically over-constrained condition can be avoided with this joint. In addition to this feature, the coupling socket joints are composed of a detachable magnetic ball and socket. When a magnetic metal ball is inserted into the socket with embedded neodymium magnets, it can be held there and rotate as a 3-DOF rotational joint. If excessive force is applied

to the proposed system from faulty control, unexpected motion error, or overload, it will automatically be detached to protect it from damage to both the robot arms and the proposed motion gauge system. The proposed motion gauge measures the displacements of the two arms along the center line of the linear rail rods, which are parallel to the line connecting the ball centers of the two robot arms. In the interest of brevity in this paper, we refer to these displacements as “linear displacements.”

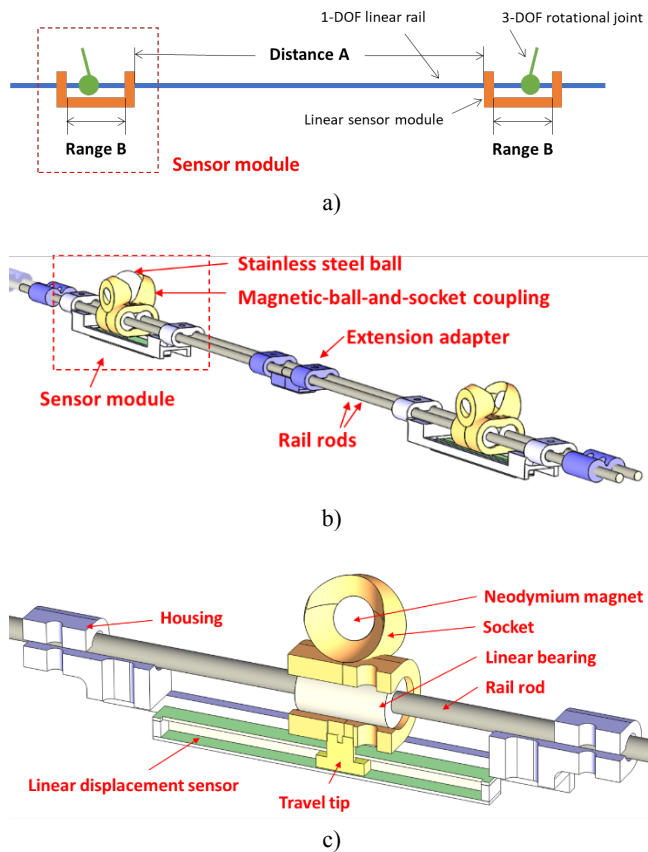


Fig.2. Designs of the proposed motion gauge system: a) a conceptual design, b) a full 3D CAD model; and c) a cross-sectional view of the sensor module.

A detailed 3D computer-aided design (CAD) image of the proposed metrology bar gauge system is illustrated in Fig.2.b and Fig.2.c. Fig.2.b shows a full view of the proposed system, consisting of two linear sensor modules and the linear rail. Fig.2.c shows a cross-sectional view of the linear sensor module to illustrate the travel tip between the 3-DOF rotational joint and the displacement measurement sensor. The potentiometer tip is inserted into a hole in the socket and slides along the linear rail by the robotic arm motion.

Once the mechanical structure is built, a wireless signal conditioning unit is attached to the linear displacement sensor to transfer the measured data to a remote computer through

wireless communication. The wireless signal conditioning unit connection diagram is shown in Fig.3.a, where each linear displacement sensor has one wireless signal conditioning unit. The first wireless signal conditioning unit gathers all the measured data from the other wireless modules and sends them to a remote computer. Three or more wireless modules can be added to the current system without any significant modification. Since it is rare to directly measure the resistance of the potentiometer, a voltage divider is utilized to measure it by converting it into a voltage output, as shown in Fig.3.b.

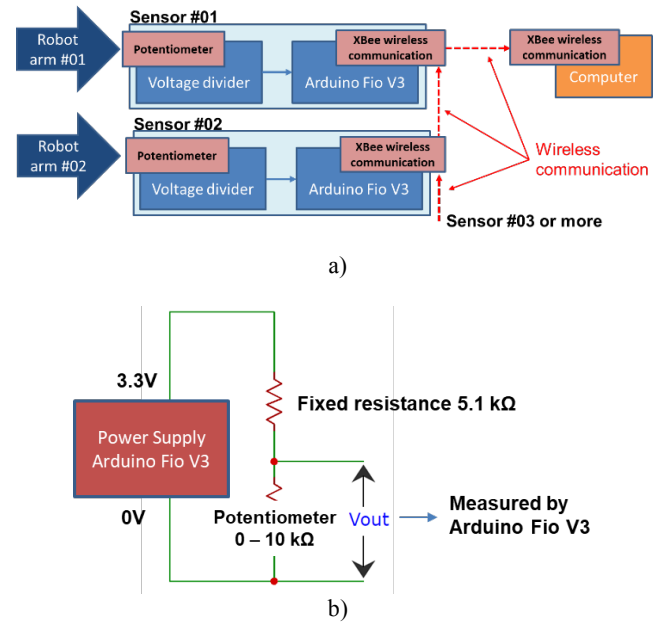


Fig.3. The wireless signal conditioning unit: a) the wireless connection diagram, and b) the voltage divider.

A. Fabrication

The metal components, such as the metal balls, neodymium magnets, and linear bearings of the proposed devices, were obtained from commercially available products. The design parameters and technical details about these components are listed in Table 1. All the non-metal components are fabricated by 3D printer MakerBot¹ Replicator 2 [15] with acrylonitrile butadiene styrene (ABS) filaments [16]. This printer can provide the positioning precision of 0.011 mm for horizontal movement and 0.0025 mm for vertical motion.

The assembled view and the detailed views of the proposed device are shown in Fig.4. and Fig.5. The sensor module in Fig.4.a shows that the potentiometer, as a linear displacement sensor, is attached under the magnetic ball-and-socket coupling, which works as a 3-DOF rotational joint. With the sensor module housing, the potentiometer is mechanically linked to the coupling. The wireless signal conditioning unit is attached to the bottom of the potentiometer and is

¹ Certain trade names and company products are mentioned in the text or identified in an illustration to adequately specify the experimental procedure and equipment used. In no case does such an identification imply recommendation or endorsement by the National Institute of Standards and

Technology, nor does it imply that the products are necessarily the best available for the purpose.

electrically wired. This unit consists of the Arduino¹ Fio V3 board [18], as a data processor, and the XBee¹ wireless communication module [21], as a data communicator. The Fio V3 board provides nine analog inputs and five analog outputs with a form factor of 25 mm x 70 mm, a driving voltage of 3.3 V, and an operating frequency of 8 MHz [18]. The XBee module has a 30-m reachable wireless range and provides good compatibility with the Fio V3 board. Both are electrically powered by the lithium-ion battery [19] placed between them. The voltage divider in Fig.3.b is implemented with an electrical resistor of 5.1 kΩ and indicated by the red box in Fig.4.a. The wireless data receiver is shown in Fig.4.b, which is linked to a remote computer through a universal serial bus (USB).

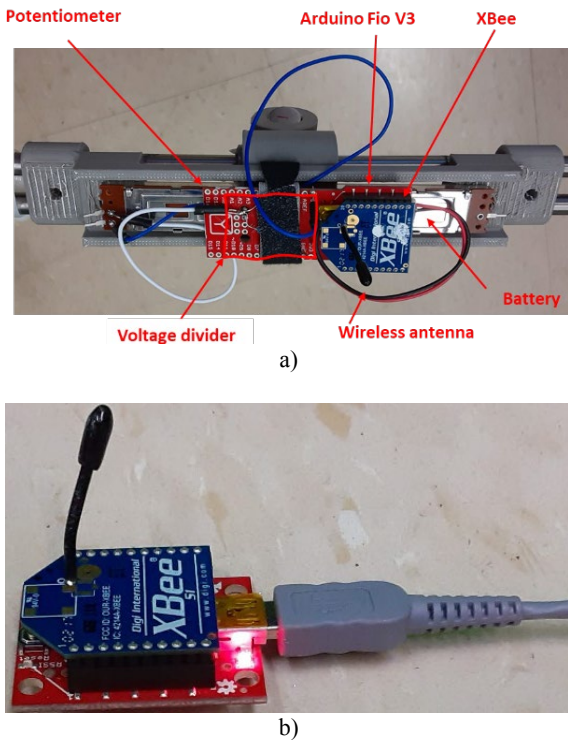


Fig.4. The sensor module: a) the sensor module with the wireless signal conditioning unit, and b) the wireless receiver module connected to a remote computer.

Table 1. Technical information of the metrology components of the sensor module.

Components	Description
Linear rail rod	1.5 m long, made of titanium
Potentiometer	Part number: PTB0143-2010BPB103, 0 – 10 kΩ, 100 mm travel range [17]
Arduino	Arduino Fio V3, 3.3 V output [18]
Battery	Polymer Lithium-Ion Battery, 3.7 V [19]
Metal balls	25.4 mm diameter, 500-B-T Stainless Steel 440C Threaded Balls [20]
XBee	Wireless module, 250kbps Max data rate, AT or API command set [21]

Fig.5. shows the fabricated system operating with the two arms of a Baxter robot [22], [23] built by Rethink Robotics Inc. The metal ball coupling adaptor in Fig.5.b is installed on the end effector of the robot. This metal ball coupling adaptor is nested in the socket of the sensor module and works as a 3-DOF rotational joint. With the two sensor modules, the robot in Fig.5.a holds the proposed gauge system, forming a closed kinematic chain.

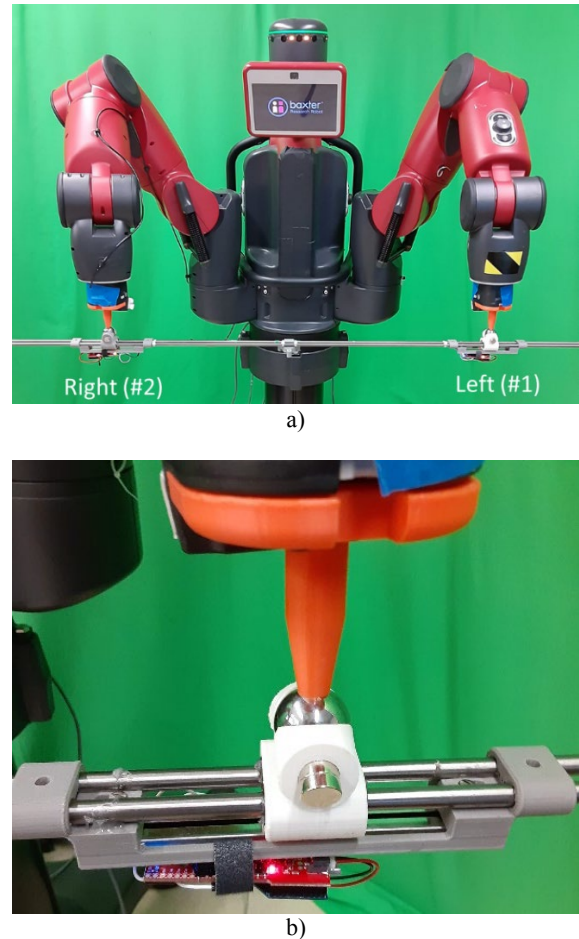


Fig.5. The fabricated Wireless Motion Gauge system: a) installed on two arms of a Baxter robot, b) the sensor module.

3. RESULTS

A. Calibration

The accuracy of the linear displacement sensor shown in Fig.2.c is measured before the displacement sensor is mounted in the motion gauge system of each sensor module. This calibration measurement was done with the Nikon¹ laser radar system MV-200 [24], because of its capability to scan spherical surfaces and find the location of the center of the sphere in 3D space. The MV-200 manufacturer claims that it can measure the coordinates of the sphere center with an accuracy of 0.024 mm at 2 m distance and 0.209 mm at 20 m distance. For the performance of this measurement with the Nikon laser radar system, a metal ball was attached to the travel tip of the sensor. By moving the travel tip from one side to the other, the center coordinates at twelve different

positions were measured by both the Nikon laser radar system and the linear displacement sensors. Both data were compared with each other, showing that these commercial products have wide variation in their performance and the linear displacement sensors currently being used have an accuracy from 0.041 mm to 0.051 mm.

The assembled motion gauge system is calibrated and evaluated to measure the distance between the two sensor modules from their linear displacement sensor electric outputs. To track the two sensor modules at the same time, the OptiTrack¹ V120: Trio motion tracker¹ [13] is utilized, which can track the reflective spheres in the sockets of the sensor modules. For this calibration, the two sensor modules were moved randomly from one side to the other twelve times and the corresponding coordinates of the twelve positions were measured, which were used for the calibration. The corresponding distance-to-outputs voltage relationship is shown in Fig.6., where a curve fitting was made by the interpolation from a 2nd order polynomial curve fitting toolbox in MATLAB¹.

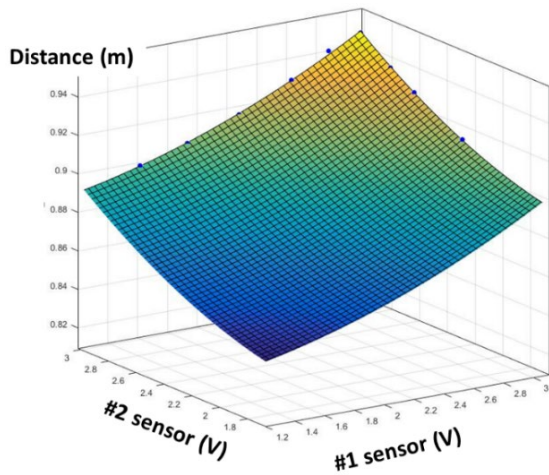


Fig.6. Calibration of the two sensor modules.

The curve fitting result by MATLAB¹ is expressed as follows:

$$Distance (mm) = 5.14P_1^2(V_1) - 12.93P_1(V_1) + 10.72P_2^2(V_2) - 60.84P_2(V_2) + 850.5 \quad (1)$$

where P_1 is the voltage output (V_1) from the left (or #1) sensor module, P_2 is the voltage output (V_2) from the right (or #2) sensor module, $1.10 \text{ V} < V_1 < 3.05 \text{ V}$, and $1.50 \text{ V} < V_2 < 2.95 \text{ V}$. The distance A in Fig.2.a is adjusted to be 830.18 mm for a Baxter robot to test, and the measurable distance of the proposed system ranges from 839.17 mm to 947.97 mm. After this calibration, the two modules were moved randomly to ten positions and the corresponding measurements were compared with the OptiTrack V120, showing that its accuracy is 0.104 mm.

B. Symmetrical Coordinated-motion task description

For the proposed system, a symmetrical coordinated-motion task was planned with a Baxter robot equipped with

two arms. As shown in Fig.7., a closed kinematic chain was formed with the two arms and the metrology bar attachment. The two arms were then programmed to move forward 200 mm along the robot X-axis and move back to their original position, as indicated by the red arrows in Fig.7. During this operation, the two arms were programmed to maintain the same distance between them, such as moving an object with the two arms gripping it from both sides.

To show the suitability of the proposed motion gauge, this 200 mm movement task was repeated with six different settings: the first setting was to move 200 mm non-stop (direct movement or zero via-point task), and the second setting added one via point. The number of via points was increased to five for the 200 mm movement. The via points are located on the imaginary line connecting the starting position and the final programmed position, with the same distance gap for each pair of via points for fine linear motion. In an ideal case, the distance between the two arms should remain unchanged during these operations. In practice, these programmed operations are not perfectly executed, and the proposed device can be used to evaluate the ability of the two robot arms to perform symmetrical coordinated motions.

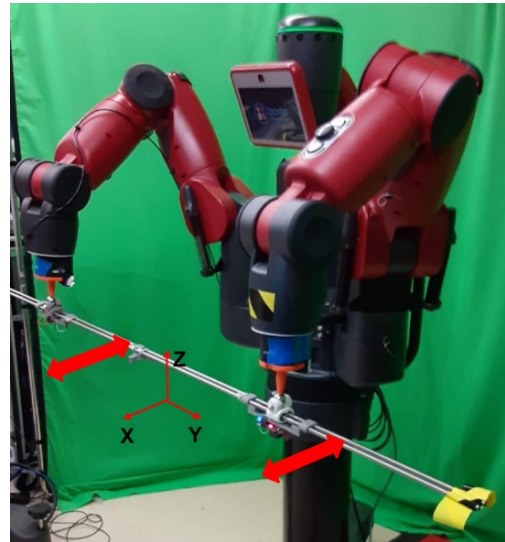


Fig.7. Experimental settings of the Baxter robot with the proposed motion gauge attached; the coordinate frame and the linear motion indicated by the red arrows.

C. Experimental results

The real-time distance between the grippers of the two moving robot arms was monitored with the proposed wireless motion gauge system during the motion tasks described in the previous section. Fig.8.a shows the recorded distance data plots of the direct movement, or zero via-point task, and the one with the four via-point task, as a function of time. The robot used in this test tended to decrease its speed around the via points for more accurate positioning. Consequently, the completion time for the task with four via points took longer than for the zero via-point task. However, the four via-point task case showed a distance change error of approximately 10 mm, while the zero via-point task case showed a distance change error of approximately 30 mm. Fig.8.b shows the

maximum distance change between the grippers of the two moving robot arms for a few test runs, as a function of the number of each task via point. Six tests were conducted: 1) no via programmed points, 2) one via point, 3) two via points, 4) three via points, 5) four via points, and 6) five via points.

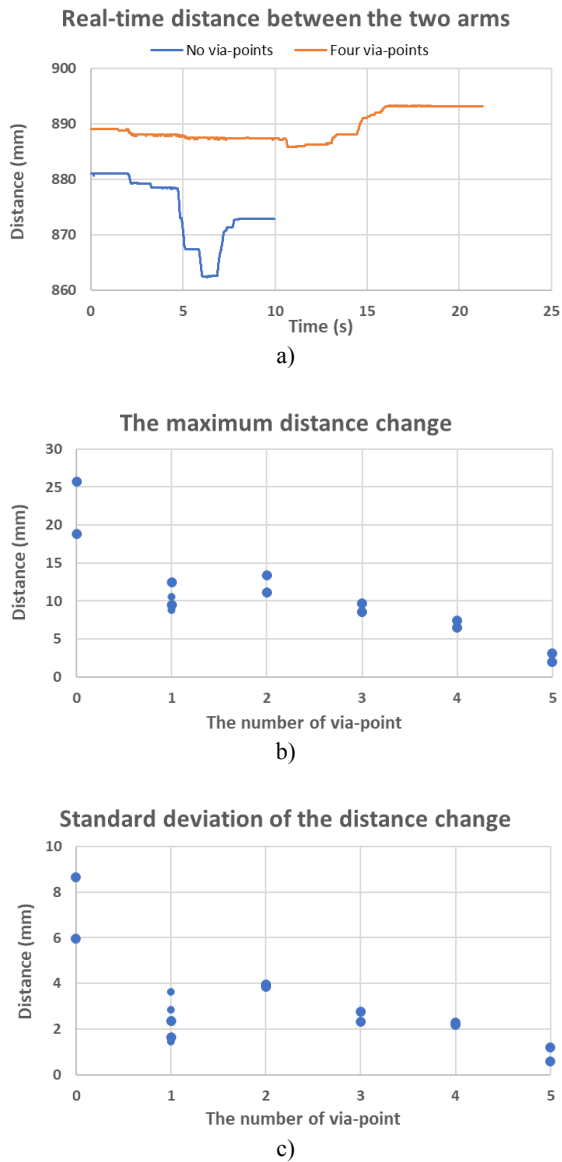


Fig.8. Distance between the two arms of a robot as measured by the proposed metrology bar gauge: a) real-time distance between the two arms, b) the maximum distance change as a function of the number of via-points, and c) the standard deviation of the distance change as a function of the number of via-points.

From this figure, we can see that increasing the number of via points resulted in a precipitous decrease in the magnitude of the maximum distance change errors. Fig.8.c is a plot of the standard deviation values of all the distance change errors of each test run as a function of the number of via points used for that run. From this plot, it is obvious that increasing the number of via points decreases the spread of distance change errors, but the price that one pays for this performance increase is a longer cycle time. The experimental data shown

in this work do not directly tell the performance of the robot used for this test, but this can show the possibility of the proposed device as a useful evaluation tool for symmetrical coordinated-motion tasks.

D. Application of the proposed system with a Hexapod

The proposed motion gauge system can extend its capability by integrating it with existing metrological systems. For this extension, a six-degrees-of-freedom (6-DOF) pose (position and orientation) hexapod measurement system is combined with the proposed motion gauge. In this case, the integrated sensor can measure the 3-DOF positions for the two robot arms, with respect to the hexapod ground-based coordinate frame.

The 6-DOF pose metrology system used for this test is based on a Stewart hexapod platform [25], [26], and it can measure the 6-DOF pose of its top platform by monitoring the length change of its six struts. The proposed motion gauge system was mounted on the top platform of the Stewart hexapod platform, as shown in Fig.9.a. The 3D position of the robot arms' coupling ball can be obtained from the 6-DOF pose of the top platform and the two sensor modules in the proposed system.

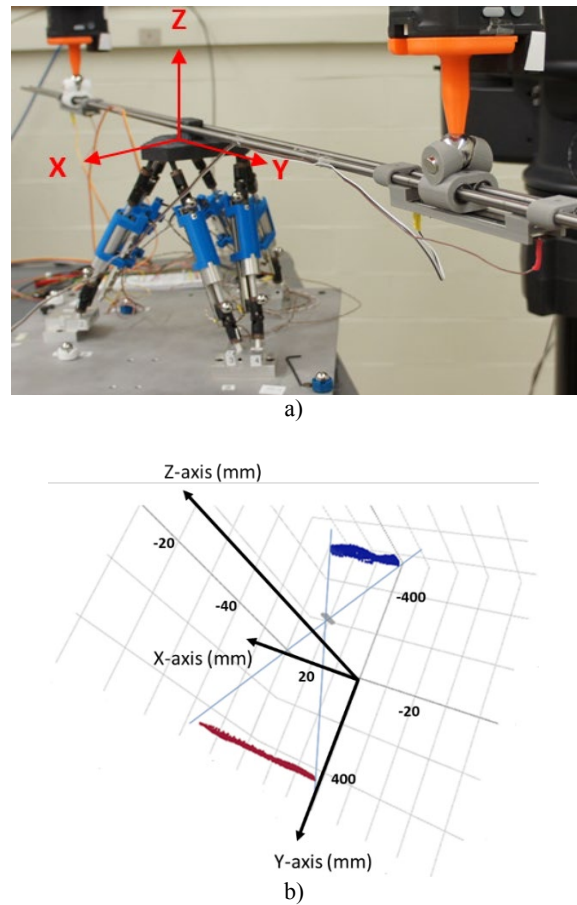


Fig.9. The metrology bar gauge mounted on an independent 6-DOF metrology system: a) The 6-DOF metrology system is based on a Hexapod Stewart platform; b) Measurement of the 3D positions of the two robot arms, while they are programmed to simulate the motions of turning a circular valve handle.

When the proposed device is attached to a stationary 6-DOF pose measurement system, its portability is not as important, so the wireless communication module and the voltage divider were replaced with a wired connection and a Wheatstone bridge. The proposed gauge was recalibrated with a Nikon¹ laser radar system MV-200 [24].

A symmetrical coordinated-motion task simulating turning a circular valve handle with two arms was performed with the two arms of a Baxter robot and was repeated several times. The corresponding 3-DOF positions of the two robot arms were measured and plotted in Fig.9.b, where the blue points represent the position of the robot arm ball attached to the left (or #1) sensor module, and the red points represent the position of the robot arm ball attached to the right (or #2) sensor module. The gray dots correspond to the middle point of the proposed motion gauge linear rods. This result shows the possibility that the proposed motion gauge system can be extended with the combination of an independent metrological system for complex measurement.

Based on the ISO9283:1998 Manipulating industrial robots - Performance criteria and related test methods [27], the experimental data were collected for the calculation of the accuracy and repeatability errors of this operation and are described in the following: The positioning distance accuracy (AD), which refers to the programmed commanded distance between the two robot arm ends (metrology gauge bar, ball and socket joints), can be obtained from equation (2), where the programmed commanded distance (D_c) is 1004.35 mm, the mean attained distance (\bar{D}) is 1008.73 mm, and the accuracy error is calculated as 4.38 mm. For these tests, the distance repeatability (RD) [27] in equation (3) as three times the measured standard deviation, is also calculated to be ± 14.93 mm after an operation of 10 cycles. The accuracy specification of the Baxter robot is quoted as ± 5 mm [23] and its repeatability is reported to range between 1.1 mm to 7.6 mm, for a single arm operation [28]. The repeatability level measured from these tests can probably be explained partially by the targets being farther away from the trunk of the robot [29], and the robot control and feedback algorithm not being well prepared to perform symmetrical tasks in two-arm coordinated motion.

$$AD = \bar{D} - D_c \quad (2)$$

$$RD = \pm 3 \sqrt{\frac{\sum_{j=1}^n (D_j - \bar{D})^2}{n-1}} = \pm 14.93 \text{ mm} \quad (3)$$

5. CONCLUSIONS

In this paper, a new motion gauge system is proposed to evaluate symmetrical coordinated-motion tasks among collaborative robots. For this purpose, a symmetrical coordinated-motion task was given to the two robot arms, which required them to maintain the same distance between them during a particular operation. The proposed system measures the linear distance of the two robot arm end effectors and calculates the distance change between them in real time. By comparing the measured distance of the proposed system with the commanded distance, the

performance of the two arms in symmetrical coordinated-motion tasks can be numerically evaluated.

The proposed motion gauge was designed with two sensor modules on linear rail rods. With this design, additional features were added: 1) for each robot arm a coupling socket of a 3-DOF rotational joint, 2) detachable magnetic-ball-and-socket couplings for easy mounting and protection from unexpected overload or motion errors, 3) wireless data communication to allow a wider range of motion tasks with fewer motion restrictions, and 4) a capability for integrating with other complementary metrological systems. The proposed motion gauge system has demonstrated its ability to measure the performance of two arms of a Baxter robot executing a symmetrical coordinated-motion task as a function of several programmed path via points.

The performance of symmetrical coordinated-motion tasks depends on time synchronization errors between the engaged robot arms and motion errors from each arm, which could be caused by electromechanical defects (stiction, backlash, encoder malfunction, etc.), calibration errors, torque or force limits, and so forth. The proposed system can call attention to robot operators to widen their robot programming scope to multiple robots in collaborative operations if performance evaluations of robots are feasible. This motion gauge system is designed for symmetrical coordinated-motion forming a kinematic chain among engaged robotic arms, to help understand the interaction among arms in the same kinematic chain. If asymmetrical coordinated-motion also formed a kinematic chain in some cases, this system could also be utilized for asymmetrical coordinated-motion tasks.

Future studies will try to identify these error sources in more detail. For this, the potentiometers used in the proposed system can be replaced with higher accuracy and resolution sensors to enhance its performance, such as high accuracy laser displacement sensors [19] or linear variable differential transformers (LVDT). Other linear displacement sensors, such as optical or magnetic linear encoders, can be used for a longer operational range. Future studies will also examine the effect of external temperature change to the operation of the motion gauges, the maximum allowable speed, maximum time life or cycle, etc.

ACKNOWLEDGMENT

The authors would like to thank Nithyananda Bhat for his support on the experiments with collaborative robots, Joseph Falco and Jonathan M. Griffin for their advices on the technical issues, and Nolan J. Brandenburg from the NIST machining shops for the fabrication of the proposed motion gauge parts. This work was supported by the Measurement Science for Manufacturing Robotics Program of the Intelligent Systems Division, Engineering Laboratory, National Institute of Standards and Technology, USA.

REFERENCES

- [1] Forlizzi, J., DiSalvo, C. (2006). Service robots in the domestic environment: A study of the Roomba vacuum in the home. In *HRI '06: Proceedings of the 1st ACM SIGCHI/SIGART Conference on Human-Robot Interaction*. New York, US: Association for Computing Machinery. <https://doi.org/10.1145/1121241.1121286>

- [2] Ritchie, M., Fioranelli, F., Griffiths, H. (2015). Micro-drone RCS analysis. In *IEEE Radar Conference*. IEEE, DOI: 10.1109/RadarConf.2015.7411926.
- [3] Marvel, J.A., Norcross, R. (2017). Implementing speed and separation monitoring in collaborative robot workcells. *Robotics and Computer - Integrated Manufacturing*, 44, 144-155. <https://doi.org/10.1016/j.rcim.2016.08.001>
- [4] Guiard, Y., Ferrand, T.T. (1996). Asymmetry in bimanual skills. In *Manual Asymmetries in Motor Performance*. CRC Press, ISBN 9780849389993.
- [5] Park, H.A., Lee, C.S.G. (2016). Dual-arm coordinated-motion task specification and performance evaluation. *IEEE/RSJ International Conference on Intelligent Robots and Systems (IROS)*. IEEE, DOI: 10.1109/IROS.2016.7759161.
- [6] Zollner, R., Asfour, T., Dillmann, R. (2004). Programming by demonstration: Dual-arm manipulation tasks for humanoid robots. In *IEEE/RSJ International Conference on Intelligent Robots and Systems (IROS)*. IEEE, DOI: 10.1109/IROS.2004.1389398.
- [7] Smith, C., Karayiannidis, Y., Nalpantidis, L., Gratal, X., Qi, P., Dimarogonas, D.V., Kragic, D. (2012). Dual arm manipulation-A survey. *Robotics and Autonomous Systems*, 60 (10), 1340-1353. <https://doi.org/10.1016/j.robot.2012.07.005>
- [8] Hutchinson, S., Hager, G.D., Corke, P.I. (1996). A tutorial on visual servo control. *IEEE Transactions on Robotics and Automation*, 12 (5), 651-670, DOI: 10.1109/70.538972.
- [9] Park, K.T., Park, C.H., Shin, Y.J. (2008). Performance evaluation of industrial dual-arm robot. In *International Conference on Smart Manufacturing Application*. IEEE, DOI: 10.1109/ICSMA.2008.4505596.
- [10] Nubiola, A., Bonev, I.A. (2013). Absolute calibration of an ABB IRB 1600 robot using a laser tracker. *Robotics and Computer-Integrated Manufacturing*, 29 (1), 236-245. <https://doi.org/10.1016/j.rcim.2012.06.004>
- [11] Bryan, J. B. (1984). *Telescoping magnetic ball bar test gage*. US Patent 4435905A. <https://patents.google.com/patent/US4435905A/en>
- [12] Nubiola, A., Bonev, I.A. (2014). Absolute robot calibration with a single telescoping ballbar. *Precision Engineering*, 38 (3), 472-480. <https://doi.org/10.1016/j.precisioneng.2014.01.001>
- [13] *Optitrack Trio: V120 motion tracking system*. (2021). <https://www.optitrack.com/cameras/v120-trio/>
- [14] Windolf, M., Gotzen, N., Morlock, M. (2008). Systematic accuracy and precision analysis of video motion capturing systems-exemplified on the Vicon-460 system. *Journal of Biomechanics*, 41, 2776-2780. <https://doi.org/10.1016/j.jbiomech.2008.06.024>
- [15] *Makerbot replicator 2 3D printer*. (2021). <https://www.makerbot.com/3d-printers/replicator-educators-edition/>
- [16] Weng, Z., Wang, J., Senthil, T., Wu, L. (2016). Mechanical and thermal properties of ABS/montmorillonite nanocomposites for fused deposition modeling 3D printing. *Materials & Design*, 102 (15), 276-283. <https://doi.org/10.1016/j.matdes.2016.04.045>
- [17] *Slide potentiometer, PTB0143-2010BPB103, 10 kOhms 0.5 W*. (2021). <https://www.digikey.com/product-detail/en/PTB0143-2010BPB103/PTB0143-2010BPB103-ND/3534166>
- [18] *Arduino board, Fio V3, ATmega32U4*. (2021). <https://www.sparkfun.com/products/11520>
- [19] *Polymer Lithium-Ion Battery – 40 mAh*. (2021). <https://www.sparkfun.com/products/13852>
- [20] *Material, stainless Steel 440C Threaded Balls, 0.5 inch diameter, hardened to Rc 58 min*. (2020). http://precisionballs.com/solid_works/PDF/THREAD_ED%20BALL.PDF
- [21] *XBee 1 mW Wire Antenna – Series 1 (802.15.4)*. (2020). <https://www.sparkfun.com/products/retired/8665>
- [22] Ju, Z., Yang, C., Ma, H. (2014). Kinematics modeling and experimental verification of Baxter robot. In *Proceedings of the 33rd Chinese Control Conference*. IEEE, DOI: 10.1109/ChiCC.2014.6896430.
- [23] *Hardware specification of the Baxter robot*. (2021). https://sdk.rethinkrobotics.com/wiki/Hardware_Specifications
- [24] *Hardware specification of the Nikon laser radar system. MV-200 and MV-331-351*. (2020). <https://www.nikonmetrology.com/en-us/product/laser-radar-mv331-351>
- [25] McInroy, J.E. (2002). Modeling and design of flexure jointed Stewart platforms for control purposes. *IEEE/ASME Transactions on Mechatronics*, 7 (1), 95-99, DOI: 10.1109/3516.990892.
- [26] Kim, Y.S., Shi, H., Dagalakis, N.G., Marvel, J., Cheok, G. (2019). Design of a six-DOF motion tracking system based on a Stewart platform and ball-and-socket joints. *Mechanism and Machine Theory*, 133, 84-94. <https://doi.org/10.1016/j.mechmachtheory.2018.10.021>
- [27] International Organization for Standardization. (1998). *Manipulating industrial robots — Performance criteria and related test methods*. ISO 9283:1998. <https://www.iso.org/standard/22244.html>
- [28] Chen, K.S. (2015). *Application of the ISO 9283 standard to test repeatability of the Baxter robot*. Thesis, University of Illinois at Urbana-Champaign, Urbana, Illinois. <http://hdl.handle.net/2142/88019>
- [29] Riemer, R., Edan, Y. (2000). Evaluation of influence of target location on robot repeatability. *Robotica*, 18 (7), 443-449. <https://doi.org/10.1017/S0263574799002337>

Received November 19, 2021

Accepted February 10, 2022